



Nanoparticle molybdenum dioxide: A highly active catalyst for partial oxidation of aviation fuels

Oscar Marin-Flores^a, Timothy Turba^b, Caleb Ellefson^b, Kang Wang^b, Joe Breit^c, Jeongmin Ahn^b, M. Grant Norton^b, Su Ha^{a,*}

^a Voiland School of Chemical Engineering and Bioengineering, Washington State University, P.O. Box 642710, Pullman, WA 99164-2710, USA

^b School of Mechanical and Materials Engineering, Washington State University, P.O. Box 642920, Pullman, WA 99164-2920, USA

^c System Concept Center, Boeing Commercial Airplanes, 6600 Merrill Creek Pkwy, Everett, WA 98203, USA

ARTICLE INFO

Article history:

Received 8 December 2009

Received in revised form 23 May 2010

Accepted 26 May 2010

Available online 2 June 2010

Keywords:

Molybdenum dioxide nanoparticles

Hydrogen production

Partial oxidation

Jet fuels

ABSTRACT

The More Electric Airplane (MEA) concept may be the most innovative development in aviation since the Wright "Flyer" and certainly represents the most transformative change in commercial aviation since the first use of jet engines in 1952. One of the key requirements for enabling the MEA is fuel-flexible solid oxide fuel cell systems that operate directly on logistics fuels such as Jet-A. Of the many fuel cell systems, a solid oxide fuel cell with an internal reforming is most interesting technology for commercial aviation due to its simplicity. In this paper, we show that nanoparticle molybdenum dioxide (MoO_2) synthesized directly from a reducing ethylene glycol/water solution can catalyze the partial oxidation of dodecane (a C-12 hydrocarbon surrogate for Jet-A fuel) at weight-hourly-space-velocities up to 10 h^{-1} . Even at these very high flow rates the MoO_2 nanoparticle catalyst shows a remarkably high fuel conversion of > 90% with a hydrogen yield of > 70% and an exceptional coking resistance. Under similar environments, conventional Ni-based catalysts and commercial low surface-area MoO_2 quickly deactivate due to coking. Our results demonstrate that in its nanoparticle form MoO_2 represents a very promising alternative to expensive noble metals for the internal reforming anode of direct Jet-A solid oxide fuel cell and is an important step towards realization of the MEA.

Published by Elsevier B.V.

1. Introduction

Growing concerns over global climate change and national energy security are requiring a reduction in the consumption of fossil fuels [1]. These concerns are greatly impacting future aircraft design and commercial manufacturers such as Boeing Commercial Airplanes are working on cleaner, quieter, and more fuel-efficient airplanes. A concept called the More Electric Airplane (MEA) will allow greater fuel efficiency by substituting hydraulically and pneumatically driven systems by those based on electrical energy [2]. The increased electrical power demand in a MEA can be met by decentralizing the power-producing units using small individual devices such as fuel cells. Furthermore, existing commercial aircraft use a low efficiency gas turbine auxiliary power unit (APU) to provide electrical power for operating navigation systems and various other electronic devices. By replacing the conventional APU with a solid oxide fuel cell (SOFC) APU, improvements can be made in providing a means to obtain auxiliary power without consuming excessive amounts of fuel when the airplane is on the ground or

when the load is increased on the main engines during flight [3]. Thus, fuel cells may become the primary electrical power source with engine-driven generators serving a backup role on future airplanes.

An important practical requirement for the use of fuel cells on commercial and military airplanes is that they must operate using kerosene-based aviation fuels (such as Jet-A and JP-8), which are already on board. The existing approach for fuel cell systems operating on Jet-A fuel (the standard kerosene-based commercial aviation fuel) requires a fuel reformation process in which the Jet-A is mostly converted to hydrogen and carbon monoxide [4–6]. This syngas mixture is fed into SOFCs where it is electrochemically converted to H_2O and CO_2 , and produces electrical power. However, a more efficient approach involves the operation of SOFCs with internal reforming. For such devices, hydrocarbon fuels are directly fed into their anodes to be internally reformed and produce syngas, which is then electrochemically oxidized by the same catalytic material to H_2O and CO_2 . To develop a high performance internal reforming anode that can operate with Jet-A fuel, a catalyst with the following attributes is required [7]:

- High oxidation activity toward Jet-A fuel
- High resistance to coking

* Corresponding author. Tel.: +1 509 335 3786; fax: +1 509 335 4806.
E-mail address: suha@wsu.edu (S. Ha).

- Stability at high operating temperatures (i.e., higher than 700 °C [8])
- High sulfur tolerance (e.g., aviation fuels typically contain 500 ppm of sulfur)
- High oxygen ion and electronic conductivities

Conventional Ni-based catalysts quickly deactivate under Jet-A fuel reforming environments due to coke formation and sulfur poisoning [9,10]. Thus, it is of extreme importance to develop new catalytic materials that can directly process Jet-A fuel.

Molybdenum dioxide (MoO_2) is a transition metal oxide that has long been known to be active for hydrocarbon decomposition [11,12] and has more recently shown to display high reforming activity for various long-chain hydrocarbons [13,14]. Marin-Flores and Ha reported that MoO_2 is highly active for reforming isoctane (a gasoline surrogate) via partial oxidation [15]. This process is exothermic ($\Delta H^\circ = -659.9 \text{ kJ/mol}$) and in the presence of MoO_2 proceeds to full conversion at 700 °C and 1 atm. The catalytic activity shown by MoO_2 can be explained in terms of the Mars-van Krevelen mechanism [16,17], which involves the consumption of nucleophilic oxygen ions provided by the oxygen sub-lattice with the purpose of sustaining the redox cycles taking place on the catalyst surface.

The capability of MoO_2 to selectively transfer lattice oxygen into hydrocarbon molecules can be attributed to the rapid formation of oxygen vacancies in its oxygen sub-lattice [18]. Consequently, MoO_2 can catalyze reactions like the carbon dioxide assisted gasification of activated carbons and chars, which would typically lead to rapid catalyst deactivation through coking [19]. Another interesting, and very relevant, feature of MoO_2 is its high sulfur tolerance. Molybdenum dioxide has been shown to maintain a high reforming activity for gasoline even in the presence of 500 ppm of model sulfur compounds [17], which is a typical concentration in most aviation fuels.

Molybdenum dioxide is also an unusual transition metal oxide because of its high metallic-like electrical conductivity ($1.1 \times 10^4 \text{ S cm}^{-1}$ at 300 K in bulk samples) [20], which is associated with its mixed interatomic bonding and a relatively high density of states at the Fermi level. The existence of free electrons in this region enhances the catalytic activity of Mo^{4+} in MoO_2 , unlike that of Mo^{6+} in MoO_3 , where all the valence electrons of the metal are covalently bonded to neighboring oxygen atoms [13]. The metallic conductivity of MoO_2 makes it a material of interest for many

applications, including catalysis. Most recently it has been studied as a possible anode for lithium-ion batteries [20].

Despite its interesting catalytic properties, a very limited number of studies have been conducted examining the potential of MoO_2 as an anode catalytic material of SOFC [19]. Such studies were carried out using commercial MoO_2 , with particle sizes in the range of a few micrometers and Brunauer, Emmett, and Teller (BET) surface areas $<10 \text{ m}^2/\text{g}$. In this paper, we report the catalytic performance of nanoparticle MoO_2 for the partial oxidation of a Jet-A fuel surrogate, *n*-dodecane ($\text{C}_{12}\text{H}_{26}$). We chose *n*-dodecane for this study because paraffinic hydrocarbons (with C between 8 and 16) constitute the most abundant components present in Jet-A fuels. By utilizing nanoparticles we have shown that it is possible to significantly increase the total reactive surface area and thus achieve reforming processes that are relevant to direct SOFC applications with much higher efficiency levels than those of commercial MoO_2 .

2. Experimental

2.1. Catalyst preparation and characterization

Nanoparticle MoO_2 was synthesized by reduction of molybdenum trioxide (MoO_3) powder in a 1:3 volume ratio of ethylene glycol to distilled water [21]. The mixture was combined in a 45 ml Teflon-lined general-purpose vessel (Parr Instrument Company), which was subsequently sealed and heated to 180 °C for 12 h. The liquid ratio of 1:3 was chosen because it yields pure single phase MoO_2 , without the need for any post-synthesis reduction. After cooling, the dark colored MoO_2 was filtered and air dried at 100 °C. It is relevant to note that the process used to produce the MoO_2 nanoparticles is scalable and large quantities of catalyst could easily be prepared.

BET surface area measurements were carried out using a Coulter SA-3100 automated characterization machine and previous degassing of the sample under vacuum at 513 K during 30 min. The morphology of the powder samples was examined using both SEM (FEI Sirion operated at 15 kV) and TEM (Philips CM-200 operated at 200 kV). X-ray diffraction patterns were obtained using the Bragg-Brentano optical configuration in a Philips diffractometer with Co K α radiation and Fe filter. XPS analysis was performed with an AXIS-165 manufactured by Kratos Analytical Inc. using an achromatic Mg K α (1254 eV) X-ray radiation with a power of 210 W.

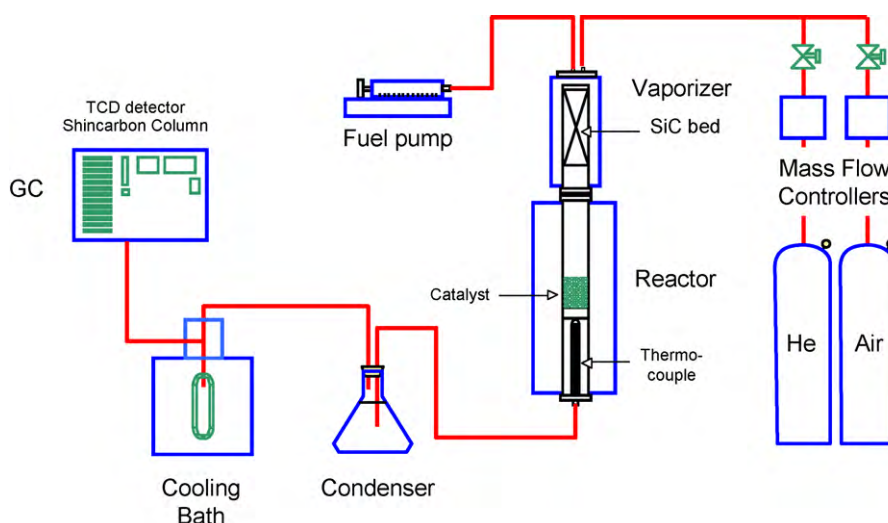


Fig. 1. Experimental arrangement for catalytic activity measurements.

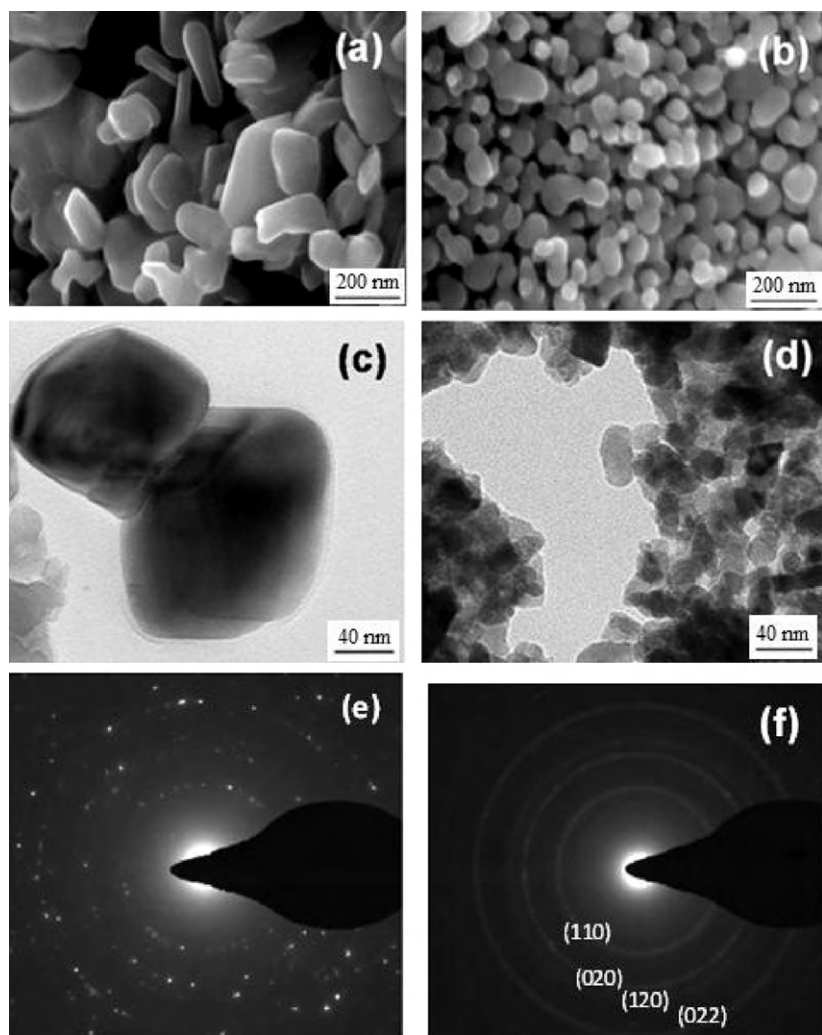


Fig. 2. SEM and TEM images of commercially available MoO_2 (a and c) and nanoparticle MoO_2 (b and d). The corresponding selected area electron diffraction patterns as shown in (e) and (f), respectively. The index of electron diffraction pattern for nanoparticle MoO_2 (f) matches to that of pure bulk MoO_2 .

2.2. Activity tests

Fig. 1 shows a schematic diagram of the experimental setup employed to measure the activity of the catalysts under partial oxidation conditions. The catalyst samples, in powder form, supported by a quartz wool plug were placed inside a 12 mm fixed-bed tubular (quartz) reactor. No catalyst pretreatment was applied prior to the activity tests. The liquid feed, consisting only of *n*-dodecane, was fed into the furnace at 500 °C, where it was vaporized and mixed with air, employed as oxygen source. A silicon carbide bed inside the furnace was used to enhance the mixing of the reactants. A calibrated syringe pump and a mass flow controller allowed the control of the flow rates of liquid fuel and air, respectively. The exit stream was cooled down to 5 °C to separate water, non-reacted fuel, and other possible condensable products from the gas product. The composition of the dry off-gas was monitored using an SRI chromatograph with a thermal conductivity detector (TCD) and a Shincarbon packed column to determine the concentrations of H_2 , CO , CO_2 , and CH_4 .

The catalytic performance was analyzed in terms of three parameters:

- H_2 yield: the ratio between the hydrogen atoms produced in the form of molecular hydrogen from the off-gas and the total amount of hydrogen atoms in the fuel stream.

- CO yield: the ratio between the carbon atoms produced in the form of the carbon monoxide and the total amount of carbon atoms in the fuel stream.
- Conversion: the ratio between the total amounts of carbon atoms produced in the form of carbon monoxide, carbon dioxide and methane and the total amount of carbon atoms in the fuel stream.

3. Results and discussion

3.1. Characterization of catalytic materials

Fig. 2 shows a montage of scanning electron microscope and transmission electron microscope images comparing commercially available MoO_2 (Alfa Aesar) with nanoparticle MoO_2 . The commercial powder consists of irregular shaped particles with a wide range of sizes. Most of the particles have diameters >200 nm, although occasionally much smaller particles were found. In contrast, the nanoparticle MoO_2 has a much more uniform particle size and shape, consisting of equiaxial particles with average size of about 20 nm. The selected area diffraction patterns (SADPs) confirm the presence of MoO_2 in both sets of powders.

Fig. 3 shows X-ray diffraction patterns obtained from both the commercially available MoO_2 and nanoparticle MoO_2 . In both cases, only the peaks for the distorted rutile structure of the dioxide phase are present. The two most intense peaks at $2\theta = 30.5^\circ$

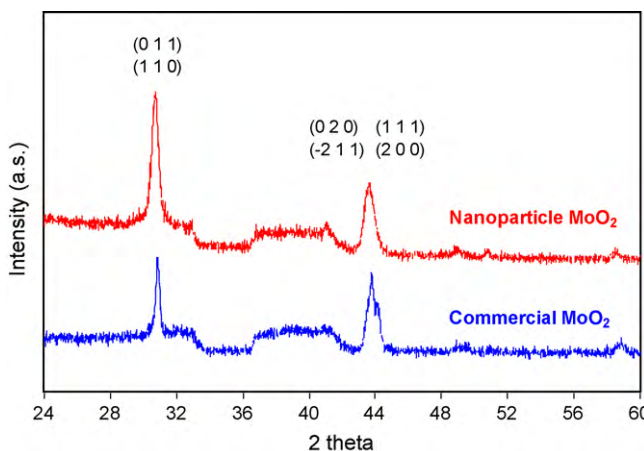


Fig. 3. XRD patterns of MoO_2 samples.

and 44.0° are due to overlapping of reflections from the (0 1 1) and (1 1 0), and (0 2 0), (-2 1 1), (1 1 1) and (2 0 0) planes, respectively. Using the Scherrer method the average particle size was determined from peak broadening to be 23 nm for the synthesized nanoparticle MoO_2 . This value is consistent with the TEM observations.

The BET surface area of the nanoparticle MoO_2 was determined to be $48 \text{ m}^2/\text{g}$, which is about an order of magnitude greater than that of the commercially available material.

3.2. Catalytic activity measurement

To investigate the catalytic activity of nanoparticle MoO_2 for the partial oxidation of *n*-dodecane, tests were conducted at 850°C and 1 atm, with a weight-hourly-space-velocity (WHSV) of 1.1 h^{-1} and an O_2/C ratio of 0.5. The process can be described by Eq. (1):



The operating temperature was chosen to prevent carbon formation since the reverse Boudouard reaction is thermodynamically favored if the operating temperature is $<700^\circ\text{C}$ [8]. The O_2/C ratio was set to 0.5 on the basis of our thermodynamic calculations, which show that ratios <0.5 promote carbon formation in the catalytic material whereas ratios >0.5 lead to an increase in the concentrations of CO_2 and H_2O as a result of complete oxidation of the fuel.

Fig. 4 shows the time-evolution of the catalytic performance of nanoparticle MoO_2 under the specified operating conditions. The

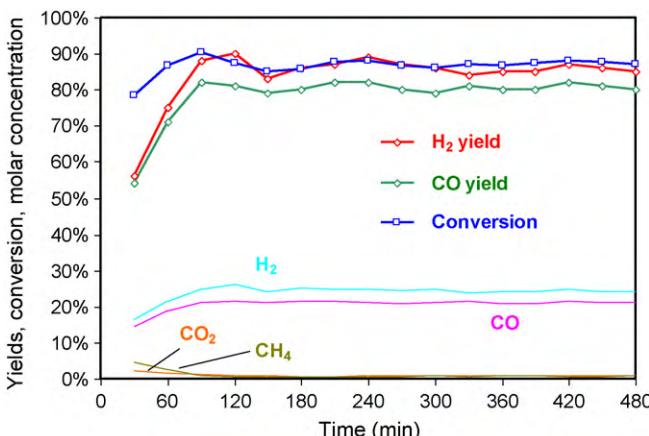


Fig. 4. Catalytic activity of nanoparticle MoO_2 for partial oxidation of *n*-dodecane.

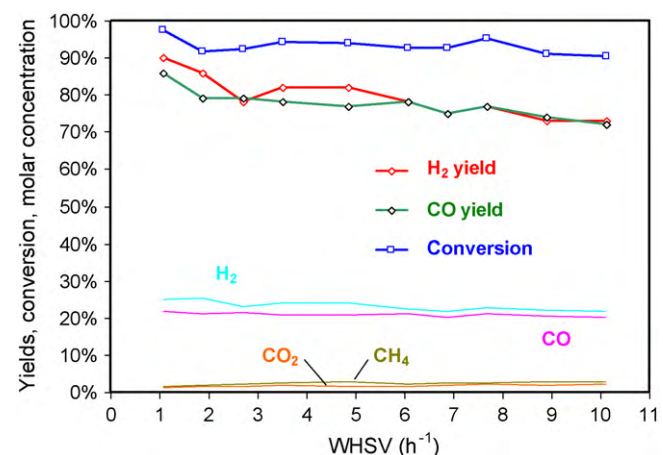


Fig. 5. Effect of fuel flow rate in terms of WHSV on the catalytic activity of nanoparticle MoO_2 .

process takes about 1 h to reach steady state conditions at which point the H_2 yield, CO yield and conversion become approximately 85%, 85% and 80%, respectively. As expected from the stoichiometry of the reaction, an O_2/C ratio of 0.5 leads to a small concentration of CO_2 whereas the concentrations of H_2 and CO attain values of about 25% and 20%, respectively. The reduced concentration of CH_4 suggests that thermal cracking of the fuel was taking place at low rates.

Fig. 5 shows the effect of the WHSV on the catalytic performance of nanoparticle MoO_2 . The operating conditions chosen for this test were the same as described above: 850°C , 1 atm, and an O_2/C ratio of 0.5. The WHSV range considered was $1\text{--}10 \text{ h}^{-1}$. As noticed, the conversion decreased from 97% to 91% as the WHSV increased from 1 to 10 h^{-1} . The H_2 yield and the CO yield gradually decreased from 90% to 73% and from 88% to 72%, respectively whereas the concentrations of H_2 , CO , CO_2 and CH_4 appeared not to be significantly affected by operation at very high flow rates, which suggests that no changes occurred in the reaction mechanism.

Fig. 6 is particularly significant because it compares the effect of WHSV, i.e., fuel flow rate, on the catalytic performance of both nanoparticle MoO_2 and commercially available MoO_2 . The H_2 production rates at equilibrium conditions determined from thermodynamic calculations have been included as a reference (i.e., the equilibrium value would represent a theoretical maximum production rate). As seen, the H_2 production rates for both catalysts are initially similar, displaying a linear increase as the WHSV was

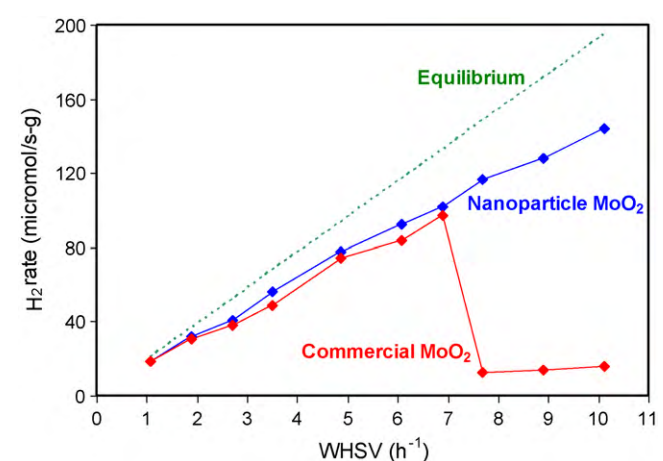


Fig. 6. Hydrogen yield as a function of WHSV.

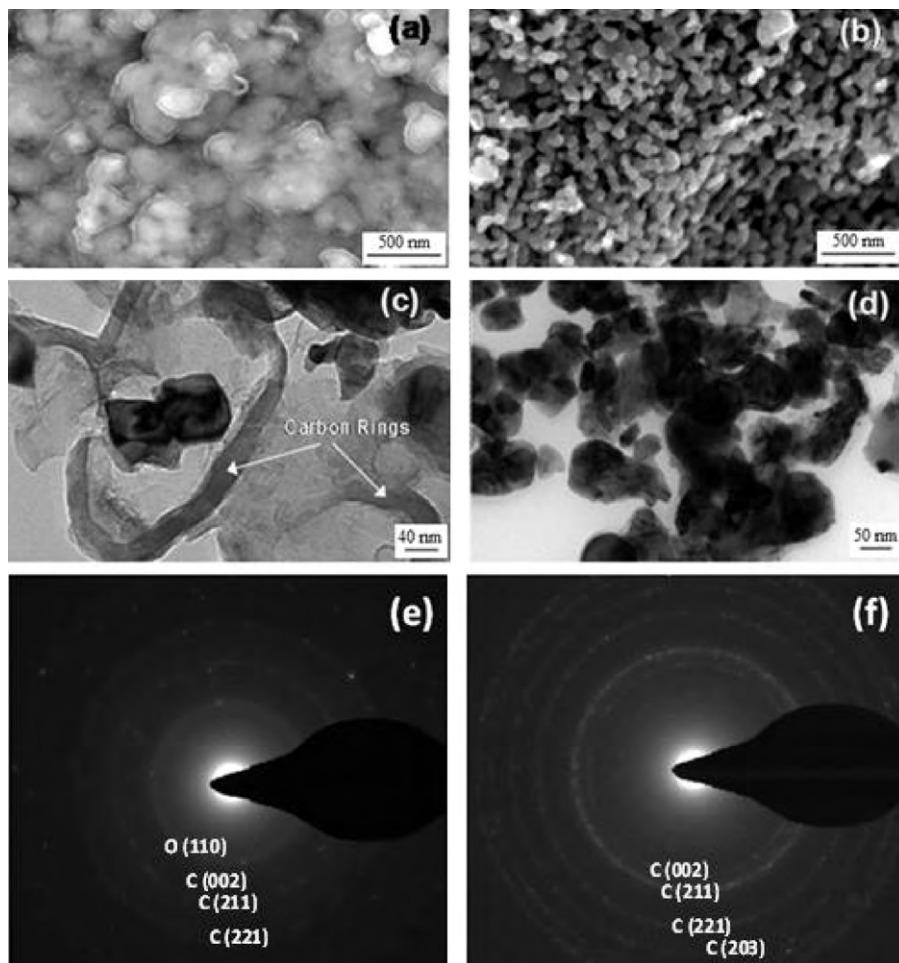


Fig. 7. SEM and TEM images of spent samples of commercial MoO₂ (a and c) and nanoparticle MoO₂ (b and d). The corresponding SADP patterns are shown in (e) and (f), where a symbol “o” stands for the index of Burke MoO₂ and a symbol “c” stands for the index of bulk Mo₂C.

increased from 1 to 7 h⁻¹; the nanoparticles give rates slightly closer to the equilibrium values. The inability of both catalytic materials to produce reaction rates closer to those at equilibrium conditions can be attributed to two factors. The first one is related to the kinetics of the reaction, this is, the time of contact between the reactants and the catalyst active sites seems to be insufficient to attain equilibrium. The second one has to do with the inherent selectivity of the catalytic material, which promotes the formation of other hydrogen-containing side products at expenses of molecular H₂. However, the activity of the commercial material exhibits a significant drop in the H₂ production rate as the WHSV becomes >7 h⁻¹, while the nanoparticle catalyst shows a continuous increase in H₂ production rates.

After reaction at large WHSVs the catalyst samples were reexamined using TEM and SEM (Fig. 7). The SEM micrograph of the spent commercial catalyst (Fig. 7a) indicates significant differences in terms of morphology comparing to its original starting mate-

rial (Fig. 1a). The TEM images show that the spent particles have become encapsulated by graphitic carbon (i.e. coking), which has caused deactivation. On the other hand, the shape and particle size of the nanoparticle MoO₂ (Fig. 7b and d) remain practically unaltered by the reforming environment even at the very high flow rates. TEM images of the MoO₂ nanoparticles show the complete absence of the graphitic carbon, i.e., there is no coking.

Selected area diffraction patterns from the reacted samples are shown in Fig. 7(e) and (f) for the commercial MoO₂ and nanoparticle MoO₂ samples, respectively. The SADP for the spent commercial catalyst shows reflections from both Mo₂C and MoO₂. However, the SADP from the nanoparticle catalyst shows reflections that can be indexed exclusively to Mo₂C (this was confirmed by XRD, which showed peaks only for Mo₂C).

The partial oxidation of liquid hydrocarbons over MoO₂ catalysts appears to follow the Mars–van Krevelen reaction mechanism. According to this mechanism, the hydrocarbon molecules are first adsorbed on the metal oxide surface. The next stage in the mechanism involves the oxidation of adsorbed hydrocarbons following an insertion of oxygen atoms provided by reduction of the metal oxide surface. The reduced metal oxide surface is re-oxidized and surface oxygen vacancies are replenished by gas-phase oxygen. This redox catalytic cycle is illustrated in Fig. 8.

In heterogeneous catalysis, the number of available surface active sites per weight of catalyst increases as the particle size decreases. Because of the very large surface area to volume ratio for nanoparticles, the high coking resistance displayed by the nanoparticle MoO₂ at high space velocities can be attributed to the existence

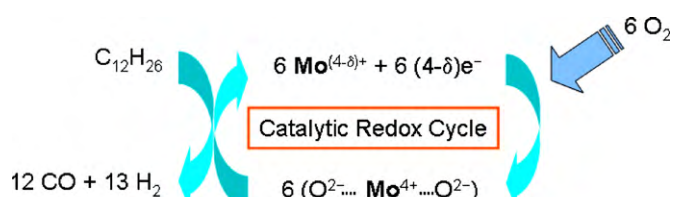


Fig. 8. The catalytic redox cycle based on the Mars–van Krevelen reaction mechanism.

of a large number of active sites available on their surface to catalytically reform the high volume of fuel into syngas. Given that the SADP and corresponding XRD analysis (not shown) of the spent nanoparticle MoO_2 sample showed only Mo_2C , then the reaction mechanism must involve the participation of only a few layers of surface oxide (i.e., there is a core–shell structure consisting of a Mo_2C core with a very thin MoO_2 shell). The presence of molybdenum carbide in the sample might be thought as responsible for the observed catalytic activity. However, to the best of our knowledge, molybdenum carbide does not promote partial oxidation of liquid hydrocarbons and, instead, Mo_2C has been found to catalyze the aromatization of liquid hydrocarbons such as *n*-octane [22]. Additionally, as part of this work, Mo_2C was tested for the partial oxidation of *n*-dodecane under the same operating conditions as those for MoO_2 and only poor activity was detected.

During the reforming reaction, the MoO_2 nanoparticles are transformed into Mo_2C through a carbothermal process that can be described as follows:



This reaction is thermodynamically favored ($K_{\text{eq}} = 1.27 \times 10^6$, at 850°C) and the mechanism of reaction has been previously investigated [23,24]. However, the mechanism of reaction involves surface MoO_2 active sites which still exist even after the whole bulk of the sample has become carbide. EDX (data not shown) supports this hypothesis since it indicates a high concentration of oxygen element which must come only from the surface/subsurface layers given that the bulk has been completely carburized. Thus, the nanoparticle surface contains enough active sites of the MoO_2 phase to sustain the surface redox catalytic cycle even at high WHSVs. A different behavior was observed for the commercial low surface area MoO_2 particles. At WHSVs $< 7\text{ h}^{-1}$, the performance was similar to that of nanoparticles. However, at WHSVs $> 7\text{ h}^{-1}$, the insufficient number of surface active sites of the MoO_2 phase could not sustain the redox catalytic cycle (Fig. 8). Thus, the rates of side gas-phase reactions become larger than that of the Mars–van Krevelen based surface reaction. These gas-phase reactions enhance the formation of methane and elementary carbon as well as that of carbon oxides. The carbon produced from these reactions then forms the shell-like structures that encapsulate the catalyst particles. This is in agreement with the particle morphology observed in the SEM and the encapsulation of particles by graphitic carbon seen in the TEM. The particle encapsulation caused by the excess carbon prevents the interaction of the hydrocarbon molecules from the fuel with the active sites located on the catalyst surface and, as a result, the catalyst performance is expected to decline. In addition, the carbon shell-like structures may prevent the diffusion of carbon into the bulk of the particles, which explains why the SADPs from these samples show reflections from MoO_2 .

The catalytic performance of nanoparticle MoO_2 was compared to those of Ni metal and a commercial rhodium-based catalyst (1% Rh in Al_2O_3). The data was obtained at 850°C , 1 atm, and an O_2/C ratio of 0.6, using actual jet A fuel purchased from the regional airport and fed into the reactor at a WHSV = 2.2 h^{-1} . The data obtained is shown in Fig. 9. As seen, under these operating conditions, unsupported nickel displays a poor performance due to rapid coking formation, which eventually plugged the reactor after only 2 h of operation. Nanoparticle MoO_2 and the rhodium-based catalyst exhibited more stable performances although with some differences in terms of selectivity. Thus, after 5 hours-on-stream, the rhodium catalyst produced higher yields of hydrogen (84.0%) and CO (80.5%), no methane and no C2 compounds. Instead, MoO_2 yielded lower yields of hydrogen (50.0%), CO (63.3%), and small concentrations of methane (2.6%) and ethylene (<0.5%) in the gas product. However, Fig. 9 also indicates that, in terms of conversion,

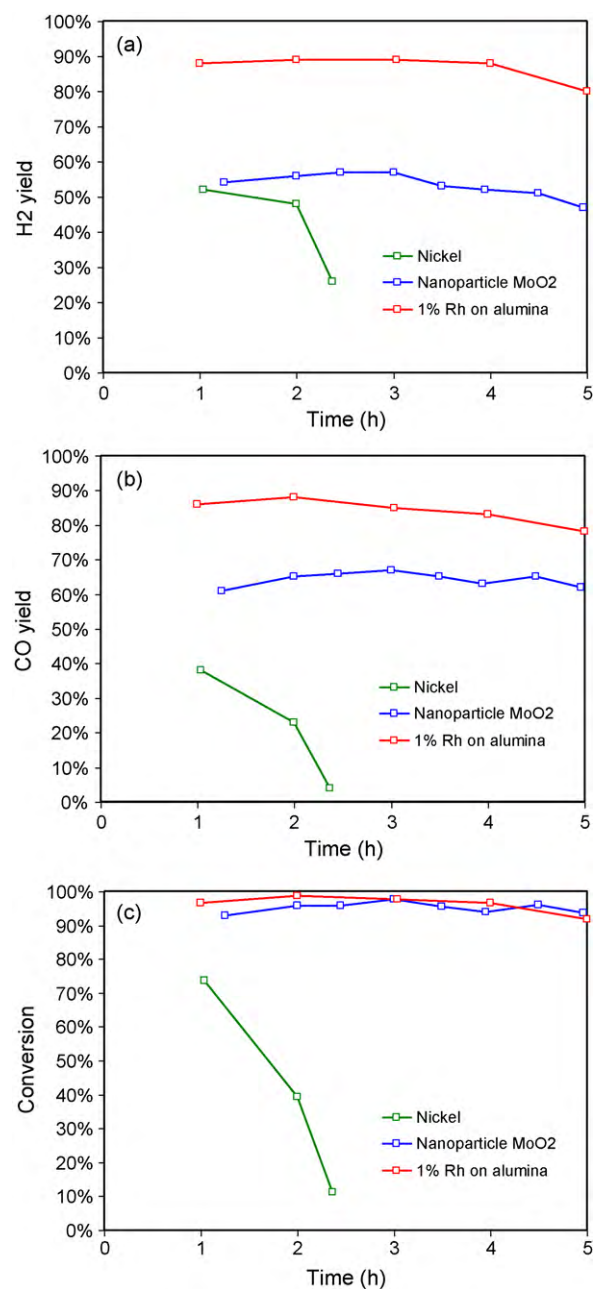


Fig. 9. (a) Comparison of H_2 yields for the partial oxidation of actual jet-A fuel: nanoparticle MoO_2 versus unsupported nickel and 1% Rh on alumina (850°C , 1 atm, $\text{O}_2/\text{C} = 0.6$, WHSV = 2.2 h^{-1}).

both catalysts displayed similar performance with values of about 94.5%.

The XRD analysis of the spent sample of nanoparticle MoO_2 indicates a barely detectable amount of MoO_2 and, instead, a significant amount of Mo_2C . On the other hand, the XPS analysis of the same sample reveals the presence of different oxidation states on the surface. In agreement with previous work [25], the presence of Mo^{2+} (carbidic Mo) was not detected; however, approximately a 20% of the Mo atoms under the oxidation state Mo^{4+} (MoO_2) and a 50% as $\text{Mo}^{2.6+}$. As concluded in the reference cited above and, in accordance with the Mars–van Krevelen mechanism of reaction, these two oxidation states are required to sustain the redox cycles taking place on the catalyst surface. These findings thus suggest a core–shell structure in the catalyst particles.

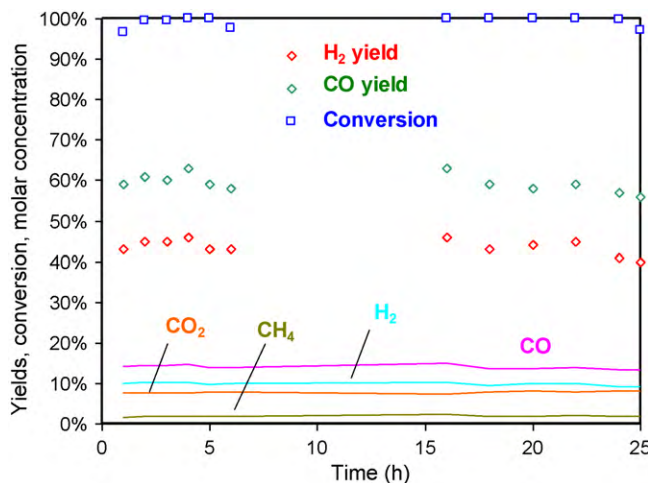


Fig. 10. Long-term performance of nanoparticle MoO₂ for the partial oxidation of actual jet A fuel (850 °C, 1 atm, O₂/C = 0.7, WHSV = 0.8 h⁻¹).

with the bulk formed by Mo₂C and the surface with the active sites (Mo⁴⁺ and Mo^{2.6+}) responsible for the catalytic activity.

An additional test was performed to measure the long-term activity of nanoparticle MoO₂ for the partial oxidation of actual jet A fuel. The operating conditions for this test were 850 °C, 1 atm, O₂/C = 0.7, and WHSV = 0.8 h⁻¹ and the results are shown in Fig. 10. As observed, after 24 h of operation, the catalyst exhibited a stable performance with H₂ and CO yields of 43.3% and 58%, respectively, and a conversion of 99.9%. The concentrations of CH₄ and CO₂ were small with values of 1.9% and 8.0%, and no C₂ compounds were detected during the test. Thus, on the basis of these results, nanoparticle MoO₂ appears to very well cope with the issues related to the use of aviation fuels, such as coking deactivation and sulfur poisoning.

4. Conclusions

In summary, the present study demonstrates that molybdenum dioxide nanoparticles possess high catalytic activity for the partial oxidation of both surrogate and actual Jet-A fuel. The coking resis-

tance and high fuel oxidation activity displayed by MoO₂ make this catalyst suitable for the reforming of various logistics fuels. In addition, the metallic-like electrical conductivity of MoO₂ allows it be used directly as an internal reforming anode in a SOFC by replacing the conventional nickel-based anode electrode. Successful development of internal reforming SOFCs using direct fuel conversion will eliminate the need for an external fuel reforming system, thereby minimizing the weight and complexity of the overall system.

References

- [1] National Academy of Sciences, *What You Need To know About Energy*. National Academic Press: Washington, D.C., 2008.
- [2] Adams, C., A380: 'More Electric' Aircraft. *Avionics* October 1, 2001.
- [3] D.L. Daggett, N. Lowery, J. Wittmann, Fuel cell APU for commercial aircraft, in: The Hydrogen Expo Conference, Hamburg, 2005.
- [4] A.F. Ibarreta, C.J. Sung, *International Journal of Hydrogen Energy* 31 (8) (2006) 1066–1078.
- [5] S. Roychoudhury, M. Lyubovsky, D. Walsh, D. Chu, E. Kallio, *Journal of Power Sources* 160 (1) (2006) 510–513.
- [6] L. Shi, D.J. Bayless, *International Journal of Hydrogen Energy* 33 (3) (2008) 1067–1075.
- [7] B.C.H. Steele, *Solid State Ionics* 86–8 (1996) 1223–1234.
- [8] Z.L. Zhan, S.A. Barnett, *Science* 308 (5723) (2005) 844–847.
- [9] M. Matsumura, C. Hirai, *Journal of Chemical Engineering of Japan* 31 (5) (1998) 734–740.
- [10] B.D. Gould, X.Y. Chen, J.W. Schwank, *Applied Catalysis a-General* 334 (1–2) (2008) 277–290.
- [11] R.H. Griffith, *Nature* 137 (1936) 538.
- [12] R.H. Griffith, *Nature* 165 (1950) 486–487.
- [13] A. Katrib, P. Leflaive, L. Hilaire, G. Maire, *Catalysis Letters* 38 (1–2) (1996) 95–99.
- [14] A. Katrib, J.W. Sobczak, M. Krawczyk, L. Zommer, A. Benadda, A. Jablonski, G. Maire, *Surface and Interface Analysis* 34 (1) (2002) 225–229.
- [15] O.G. Marin-Flores, S. Ha, *Catalysis Today* 136 (3–4) (2008) 235–242.
- [16] M.A. Vannice, *Catalysis Today* 123 (1–4) (2007) 18–22.
- [17] O.G. Marin-Flores, S. Ha, *Applied Catalysis a-General* 352 (1–2) (2009) 124–132.
- [18] W.H. McCarroll, *Solid State Chemistry Encyclopedia of Inorganic Chemistry*, vol. 6, John Wiley & Sons, New York, 1994.
- [19] F. Carrasco-Marin, J. Riverautrilla, E. UtreraHidalgo, C. Morenacastilla, *Fuel* 70 (1) (1991) 13–16.
- [20] Y. Shi, B. Guo, S.A. Corr, Q. Shi, Y.-S. Hu, K.R. Heier, L. Chen, R. Seshadri, G.D. Stucky, *Nano Letters* (2009), doi:10.1021/nl902423a.
- [21] X.Y. Chen, Z.J. Zhang, X.X. Li, C.W. Shi, X.L. Li, *Chemical Physics Letters* 418 (1–3) (2006) 105–108.
- [22] A. Szecsenyi, F. Solymosi, *Applied Catalysis a-General* 306 (2006) 149–158.
- [23] S. Chaudhury, S.K. Mukerjee, V.N. Vaidya, V. Venugopal, *Journal of Alloys and Compounds* 261 (1–2) (1997) 105–113.
- [24] M. Patel, J. Subrahmanyam, *Materials Research Bulletin* 43 (8–9) (2008) 2036–2041.
- [25] O.G. Marin-Flores, L. Scudiero, S. Ha, *Surf. Sci.* 603 (2009) 2327–2332.